THE JOURNAL OF PHYSICAL CHEMISTRY C

Article

Cite This: J. Phys. Chem. C 2019, 123, 20567−20578

pubs.acs.org/JPCC

Perylene Diimide-Based Hj- and hJ-Aggregates: The Prospect of Exciton Band Shape Engineering in Organic Materials

April Oleson,[†,⊥] Tong Zhu,[‡,§,⊥] Ian S. Dunn,[∥] David Bialas,[†] Yu Bai,[‡] Wenqing Zhang,[‡] Mingji Dai,[‡] David R. Reichman,[∥] Roel Tempelaar,[∥] Libai Huang,[‡] and Frank C. Spano*[,†]

[†]Department of Chemistry, Temple University, Philadelphia, Pennsylvania 19122, United States

[‡]Department of Chemistry, Purdue University, 560 Oval Drive, P.O. Box 68, West Lafayette, Indiana 47907, United States

[§]Laser Micro/Nano Fabrication Laboratory, School of Mechanical Engineering, Beijing Institute of Technology, Beijing 100081, P. R. China

[∥]Department of Chemistry, Columbia University, 3000 Broadway, New York, New York 10027, United States

Supporting Information

ABSTRACT: The exciton band dispersion in π-stacks of conjugated organic chromophores is a critical factor in determining the photophysical response and transport properties. In such stacks, the exciton band width and, in particular, the curvature at the band center, is determined by an interference between short-range coupling due to wave function overlap and long-range Coulomb coupling arising from transition dipole−dipole interactions. The interference can be completely destructive, yielding a dispersionless "flat" band resulting in an unusual situation where the aggregate displays monomer-like properties, despite having closely spaced chromophores. Coupled chromophores such as these are called "null aggregates" and the perfect balance of interactions that leads to them are referred to as "null points". Here, we study two perylene diimide (PDI) derivatives where positive long-range coupling induces H-aggregate behavior, whereas counteracting short-range coupling induces J-aggregate behavior. As such, both derivatives display so-called HJ-aggregate properties but are shown here to straddle a null point. In *N*-phenyl PDI π-stacks, the stronger Coulomb coupling tilts the scales in favor of overall H-like behavior resulting in Hj-aggregates, characterized by a weak 0−0 vibronic photoluminescence (PL) peak, which increases with temperature. By contrast, in tetraphenyl PDI π-stacks, the short-range coupling dominates, resulting in hJ-aggregates, as characterized by dominant 0−0 emission. Furthermore, in tetraphenyl PDI, the 0−0/0−1 PL ratio remains approximately twice the monomer value, independent of temperature, indicating strong Peierls-like dimerization. Identifying the null points in PDI derivatives provides reference geometries for band shape engineering through, for example, chemically induced or pressure-induced changes in molecular packing.

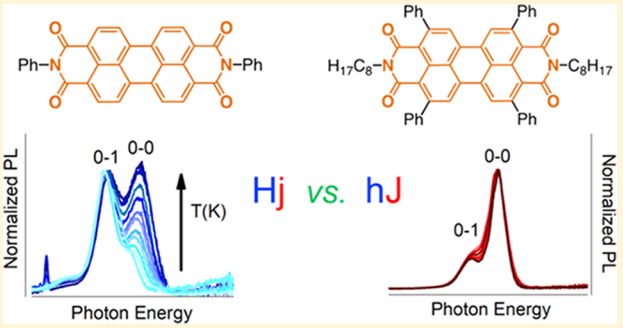

I. INTRODUCTION

Employing organic molecular and polymeric materials for electronic device applications such as solar cells and light-emitting diodes has been an area of intense activity over the past several decades.[1−7] By now, it is widely appreciated that optimal performance requires efficient design strategies that go beyond the properties of the individual molecular units and include factors related to sample morphology and, most importantly, intermolecular interactions.[8] The ability to control the properties of the exciton bands (exciton band shape engineering) is particularly appealing since the band shape impacts exciton transport as well as important photophysical properties such as the optical gap and radiative cross-section. In particular, the band width dictates the speed at which an exciton can travel, with the curvature at the band center ($k = 0$) related to the inverse of its effective mass. The sign of the curvature also dictates the photophysical properties; as first recognized by Kasha,[9−11] when the curvature is positive, the bright ($k = 0$) exciton lies at the bottom of the band as in the strongly emissive J-aggregates, whereas a negative curvature places the bright state at the top of the band as in the weakly emissive H-aggregates. The ability to engineer and control the shape of the exciton band is, therefore, enormously useful for the design of efficient organic light-emitting diodes (OLEDs) and solar cells.

One of the most versatile classes of molecules for the design of optoelectronics is the ubiquitous rylenes,[12,13] which include the numerous perylene diimide (PDI) derivatives.[13−17] Such chromophores have been extensively investigated as efficient electron-transport materials for transistor applications[17,18] as

Received: May 9, 2019
Revised: July 17, 2019
Published: August 7, 2019

DOI: 10.1021/acs.jpcc.9b04429
J. Phys. Chem. C 2019, 123, 20567−20578

well as materials for singlet exciton fission.[19−21] PDIs can assemble to form both H- and J-aggregates[22−24] based mainly on aggregation-induced spectral shifts (red-shift for J-aggregates and blue-shift for H-aggregates) consistent with the Kasha theory.[9−11] Ghosh et al.[22] demonstrated the control of H- and J-type π-stacking by tuning the peripheral alkyl side chains. Transformations between H- and J-aggregate morphologies involving the same PDI have also been observed by several groups[23,24] by disrupting H-bond formation via control of the solvent or chemical additives.

Kasha-based design schemes are predicated entirely on the intermolecular Coulomb coupling, which is generated primarily by transition dipole−dipole interactions. For example, in a linear aggregate exhibiting a "side-by-side" orientation of transition dipoles, the dominant [nearest-neighbor (n.n.)] Coulomb coupling is positive, $J_{Coul} > 0$, resulting in the bright Frenkel exciton ($k = 0$) residing at the top of the exciton band, as defines H-aggregates. Conversely, in the "head-to-tail" orientation the Coulomb coupling is negative, $J_{Coul} < 0$, so that the bright exciton resides at the band minimum, as is characteristic of J-aggregates.[9−11] Such a scheme is, however, incomplete in π-stacked systems where close intermolecular contacts enable intermolecular charge transfer (CT). Here, CT gives rise to a short-range superexchange coupling, which can be competitive with Coulomb interactions but with very different dependencies on the intermolecular geometry.[25] The simultaneous presence of both coupling sources allows for a richer array of aggregate types denoted as HJ, HH, JH, and JJ, where the first letter indicates the influence of the Coulomb coupling, whereas the second letter indicates the influence of the CT-mediated coupling.[25−29] One can also employ lower- and upper-case letters to denote relative magnitudes. The interference between the two coupling sources can be constructive (HH, JJ) or destructive (HJ, JH). For applications such as OLEDs requiring large exciton bandwidths and large emission cross-sections, JJ-aggregates are desirable, whereas for organic photovoltaic applications, HH-aggregates would be preferable since efficient solar cells require rapid excitation transport with minimal radiative loss, with the added potential benefit of reduced exciton−exciton annihilation.[30] Thus far, the destructive interference characteristic of HJ-aggregation has been observed in 7,8,15,16-tetraazaterrylene (TAT),[26,28,31,32] which forms π-stacked nanopillars when deposited on a graphitic surface.[26,31,32]

The most dramatic example of short- and long-range coupling interference occurs in the so-called "integrated" null aggregate where the cancellation is nearly complete, resulting in a flat exciton dispersion band and monomer-like photophysical properties.[29] Recently, null-dimers have been discovered in perylene diimide foldamers.[33] However, the destructive interference can also occur between positive and negative Coulombic couplings in two-dimensional aggregates, such as those composed of lutein diacetate.[29,34] In such "segregated" null aggregates, the cancelation exists only for the $k = 0$ (bright) exciton, so that it appears in the center of the band, instead of the band extremums, such as in H and J-aggregates (a detailed discussion of integrated and segregated null aggregates can be found in ref 29). Identifying null points in integrated null aggregates is of crucial importance for band shape engineering; at null points, the band is flat and, thus, a "blank canvas" from which to design bands of positive curvature (i.e., Jh, hJ, or JJ) or negative curvature (i.e., Hj, jH, or HH) depending on the desired goal.

In this paper, we investigate the photophysical properties of two perylene diimide (PDI) derivatives, namely, *N*,*N*′-bis(phenyl) PDI (*N*-phenyl PDI) and *N*,*N*′-bis(*n*-octyl)-2,5,8,11-tetraphenyl PDI (tetraphenyl PDI). The crystal structures of both derivatives are based on π-stacks but with slight differences in the slip−stack orientations, as depicted in Figure 1. Such differences result in dramatic changes in the photophysical response, which allow us to unequivocally classify *N*-phenyl and tetraphenyl PDI π-stacks as Hj and hJ-aggregates, respectively, based on their spectral signatures.[35] Importantly, each derivative lies close to a particular null point but resides on opposite sides of the balance between short- and long-range couplings. In particular, in *N*-phenyl PDI aggregates, the Coulomb coupling is slightly dominant (Hj), whereas in tetraphenyl PDI aggregates, the short-range CT-mediated coupling is dominant (hJ). We show that temperature-dependent photoluminescence (PL) provides a reliable means for determining the proximity and bias relative to a particular null point, information that is vital in design strategies for band shape engineering.

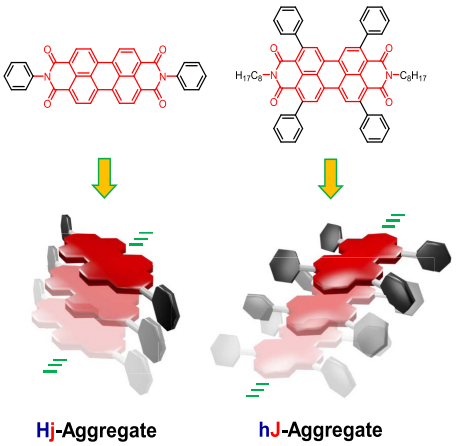

Figure 1. Molecule structures of *N*-phenyl PDI (left) and tetraphenyl PDI (right). Also shown is the π-stacking organization of both chromophores in the crystal state, as determined from X-ray diffraction. *N*-Phenyl PDI is slipped along the short molecular axis, whereas tetraphenyl PDI is slipped along the long molecular axis.

II. HJ-AGGREGATES IN PDI π-STACKS

In this section, we briefly introduce the general theoretical basis for identifying null points and aggregate types from photophysical signatures, which enable one to disentangle the relative influences of long-range Coulombic coupling and short-range CT-mediated interactions in π-stacks of PDI chromophores. As is shown below, the most sensitive probe is the temperature-dependent PL line shape, which harbors a pronounced vibronic progression in the main vinyl-stretching mode with energy 0.174 eV. In particular, the 0−0/0−1 intensity ratio can accurately track the short- and long-range coupling interference through the null point, the point at which the exciton band becomes dispersionless or "flat". In previous works,[25−27,29] hybrid aggregates have been discussed in the nonresonant regime, where high-energy CT states are treated virtually leading to an effective superexchange coupling, as well as in the resonant regime, where the diabatic Frenkel

DOI: 10.1021/acs.jpcc.9b04429
J. Phys. Chem. C 2019, 123, 20567−20578

and CT exciton bands are close in energy. It is the latter regime that best applies to the PDIs investigated herein.

As established in several works,[25,27,29,36−40] short- and long-range couplings lead to excited states consisting of an admixture of Frenkel excitons and CT excitons. For a linear aggregate (i.e., π-stack) with one molecule per unit cell, Frenkel exciton dispersion, $E_F(k)$, is dictated by the intermolecular Coulombic coupling

$$E_F(k) = E_{S_1} + \sum_n J_{mn} \cos[k(m-n)] \quad (1)$$

where k is the (dimensionless) exciton wave vector ranging from $-\pi$ to π. E_{S_1} is the energy of a chromophore locally excited in its first excited singlet state (including the gas-to-crystal shift) and J_{mn} is the Coulombic coupling between chromophores m and n, which generally derives from the atomic transition charge densities on each chromophore.[41,42] However, in tightly packed π-stacks, a locally excited state can also undergo charge transfer, as dictated by the electron and hole CT integrals, t_e and t_h, which derive from efficient LUMO−LUMO and HOMO−HOMO overlaps, respectively, between neighboring chromophores. (Here, LUMO denotes the lowest unoccupied molecular orbital, and HOMO denotes the highest occupied molecular orbital). In the simplest picture, the resulting charge-separated states are limited to nearest neighbors with energy E_{CT}. When such "diabatic" (i.e., before mixing) CT states lie sufficiently above the Frenkel band (compared to $|t_e|$ and $|t_h|$), they can be treated perturbatively, as virtual excitations, which mediate a short-range superexchange coupling, J_{CT}[25−29,43]

$$J_{CT} = \frac{-2t_e t_h}{E_{CT} - E_{S_1}} \quad (2)$$

The short-range coupling J_{CT} simply adds to the Coulomb coupling in a Frenkel-like Hamiltonian, thereby establishing a direct interference between the two coupling types in determining H- and J-like behavior.[25,27] Equation 2 shows that a positive (negative) sign for the product, $-t_e t_h$, promotes H-aggregate (J-aggregate) behavior. Figure 2 demonstrates the strong sensitivity of the product $-t_e t_h$ to molecular packing in a perylene dimer based on first-principles density functional theory (DFT) calculations. The rapid oscillations in the sign are responsible for the unusual non-Kasha geometries expected for short-range-coupled J- and H-aggregates.[25,29] For comparison, Figure 2 also shows the Coulomb coupling, J_{Coul}, derived from atomic transition charge densities,[44] which varies over much larger length scales. The yellow circle and star on each plot indicate the native orientations appropriate for *N*-phenyl PDI and tetraphenyl PDI, respectively, as determined from the crystal structure (see Section IV). Interestingly, both aggregates would be defined as H-aggregates based on the Coulomb coupling alone.

For many PDI derivatives, like the ones in the current study, the diabatic Frenkel and CT bands are sufficiently close in energy such that the superexchange picture just described is no longer valid. CT excitations need to be incorporated directly into the Hamiltonian (and not treated virtually). In the resonant regime, oscillator strength is distributed over two mixed Frenkel−CT bands. For linear aggregates (with 1 molecule/unit cell), this can be appreciated from the general dispersion relation obtained in the absence of vibronic coupling[27]

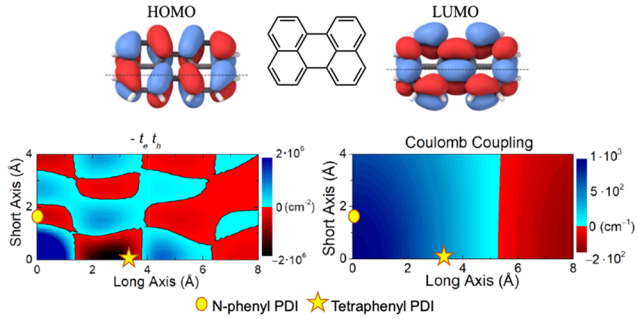

Figure 2. HOMO and LUMO orbitals of the perylene core in PDI. Left (bottom) contour plot shows the DFT-calculated values of the product, $-t_e t_h$, as a function of transverse and longitudinal displacement between two perylene molecules separated by 3.5 Å. The red regions are J-like, whereas the blue are H-like. The right (bottom) plot shows the time-dependent TDDFT-calculated *unscreened* Coulomb couplings based on atomic transition charge densities, with the energy scale corrected from ref 25. The yellow circle (star) indicates the relative orientations of the perylene cores in *N*-phenyl PDI (tetraphenyl PDI) chromophore, as determined from their crystal structures. DFT and TDDFT calculations employ the B3LYP functional. Adapted with permission from ref 25. Copyright (2017), American Chemical Society.

$$E_{\pm}(k) = \frac{1}{2}(E_{CT} + E_F(k)) \pm \sqrt{\left(\frac{E_{CT} - E_F(k)}{2}\right)^2 + 2(t_e^2 + t_h^2 + 2t_e t_h \cos k)} \quad (3)$$

Here, $E_A(k) \equiv E_-(k)$ and $E_B(k) \equiv E_+(k)$ correspond to the dispersion of the lower- and higher-energy bands, labeled A and B, respectively, which are responsible for the two-band absorption line shape displayed in the crystalline/aggregate phase of the PDI derivatives in this work (see the following section).[45] Equation 3 reduces to the diabatic CT and Frenkel exciton bands when $t_e = t_h = 0$. Equation 3 also reduces to the superexchange limit when the diabatic Frenkel and CT bands are far removed energetically.[25,27,29] Moreover, since the low-energy band A is responsible for emission (via Kasha's rule[46]), its shape determines H- and J-aggregate behavior. In particular, the curvature of band A depends on the curvature of the Frenkel band in eq 1 as well as the sign of the product, $-t_e t_h$. Hence, an in-phase relationship between t_e and t_h (such that $-t_e t_h < 0$), as exists for the two PDI chromophores in the present study (see Figure 2), induces a more positive curvature at $k = 0$. In other words, the in-phase relationship between t_e and t_h induces J-aggregate behavior. This is easiest to appreciate from eq 3 in the limit of no Coulomb coupling. Inserting $E_F(k) = E_{S_1}$ into eq 3 and applying the resonance condition ($E_{CT} \approx E_{S_1}$) leads to

$$E_A(k) \approx E_{S_1} - \sqrt{2(t_e^2 + t_h^2 + 2t_e t_h \cos k)}$$

for the dispersion of band A. The $k = 0$ exciton has the lowest energy (and the curvature is positive) when t_e and t_h are in-phase (J-like). The further inclusion of a positive (H-like) Coulomb coupling in eq 3 has the opposite effect, reducing the curvature so that the final curvature depends on the competition between short- and long-range coupling influences. Interestingly, when the two coupling sources are perfectly balanced, a flat-band results. Use of eq 3 with the nearest-

DOI: 10.1021/acs.jpcc.9b04429
J. Phys. Chem. C 2019, 123, 20567−20578

Table 1. Calculated Electron and Hole Transfer Integrals and Unscreened Coulombic Couplings for Both PDI Derivatives, Reported in cm^{-1} [a]

		t_e	t_h	J_1	J_2	J_3	J_4	J_5
N-phenyl PDI		994	392	1089	400	176	90	51
tetraphenyl PDI	1	1316	953	457	59	−2.2	−9.1	−4.9
	2	714	266	454	59	−1.5	−9.1	−4.4

[a]Electron and hole integrals were evaluated using DFT with the B3LYP functional and cc-pVDZ basis set (Gaussian 16W) using the polarization-including procedure described in ref 62. Coulomb couplings were evaluated from transition densities calculated using RPA-TDDFT with omega-B97X/ma-def2svp (ORCA). The Coulomb coupling designated J_n corresponds to the *n*th nearest-neighbor interaction along a π-stack. The "1" and "2" rows for tetraphenyl PDI indicate that interactions are taken with respect to the first or second molecule in the unit cell. All calculations were done in the gas phase using the crystal geometries and including all substituents.

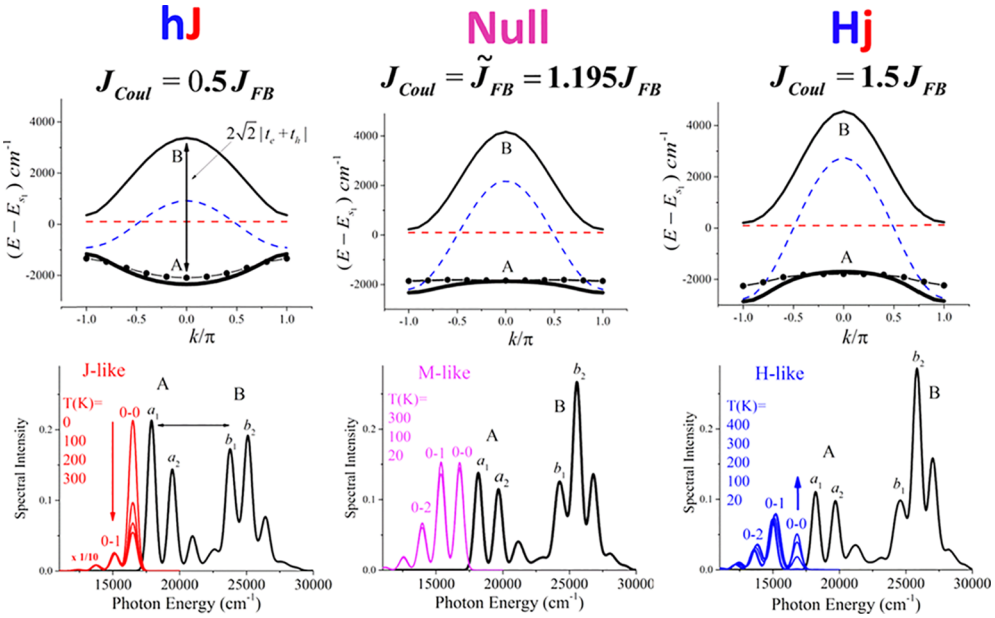

Figure 3. (Top) A and B band dispersions (black) from eq 3 for π-stacks having one molecule per unit cell with in-phase values of the CT integrals, t_e = 1200 cm^{-1} and t_h = 800 cm^{-1} and taking $E_{CT} = E_{S_1}$. The dashed lines are the diabatic CT (red) and Frenkel exciton bands (blue). The nearest-neighbor Coulombic coupling, J_{Coul} is positive (H-like), increasing from the left to right panel (J_{FB} = 920 cm^{-1} using eq 4). The solid dots represent the dispersion of band A in the presence of vibronic coupling (ω_{vib} = 1400 cm^{-1}, $\lambda^2 = 1$). Note the vibronic A band is flat in the middle panel when $J_{Coul} = \tilde{J}_{FB}$. The aggregate type is hJ (Hj) when J_{Coul} is less than (greater than) $\tilde{J}_{FB}$ (Bottom) corresponding 10-mer absorption (black) and PL spectra (red, purple, blue) calculated using eqs S.9 and S.12 assuming a monomer transition with E_{S_1} = 20 000 cm^{-1} and using the Frenkel−CT Hamiltonian in eq S.1. To more easily gauge the oscillator strength distribution among the peaks, the ω_i dependence of the oscillator strength was suppressed in eq S.10 and the cubic frequency dependence was suppressed in eq S.12. Note that the PL spectra have been shifted by one vibrational quantum to the red for clarity (otherwise, the 0−0 PL peak overlaps the absorption a_1 peak). Finally, the "superradiant" PL spectrum in the left panel (red) is scaled by a factor of $1/N$ (=1/10).

neighbor (n.n.) form of $E_F(k)$ from eq 1, $E_F(k) = E_{S_1} + 2J_{Coul}\cos k$, shows that band A becomes dispersionless when the n.n. Coulomb coupling, J_{Coul}, assumes the "flat-band" value, J_{FB},[27] with

$$J_{FB} = \frac{4t_e t_h}{(E_{CT} - E_{S_1}) + \sqrt{(E_{CT} - E_{S_1})^2 + 8(t_e^2 + t_h^2)}} \quad (4)$$

Equation 4 represents the null-aggregate condition in the absence of vibronic coupling (see below). Using physically relevant values of $t_e = t_h = 10^3$ cm^{-1} and assuming $E_{CT} \approx E_{S_1}$, gives J_{FB} = 250 cm^{-1}, which is in line with the calculated screened n.n. Coulombic interactions in perylene and PDI chromophores, obtained from the unscreened values in Figure 2 and Table 1 after dividing by the relative dielectric constant, $\varepsilon \approx 3-4$.

Figure 3 shows how increasing the n.n. Coulomb coupling, J_{Coul} (with $J_{Coul} > 0$, i.e., H-like), in a π-stack with in-phase t_e/t_h values reduces the curvature of band A, leading eventually to band inversion and a conversion from hJ- to Hj-aggregate behavior. Band A is shown without vibronic coupling (solid black curves) using eq 3 and with vibronic coupling in a 10-mer stack (black dots) assuming ω_{vib} = 1400 cm^{-1}, which corresponds to the vinyl-stretching mode observed in virtually all PDI derivatives and taking the Huang−Rhys (HR) factor to be unity, $\lambda^2 = 1$. The black dots comprising band A in Figure 3 were evaluated using the full Frenkel−CT/Holstein Hamiltonian analysis [see the Supporting Information (SI)]. Figure 3 shows that when the Coulomb coupling is relatively weak (left panel), the curvature of A remains positive, independent of vibronic coupling, due to the dominance of Frenkel−CT coupling, resulting in a hJ-aggregate. Further increasing J_{Coul} results in a flat band, shown in the center panel of Figure 3, for band A in the presence of vibronic coupling. This requires a value of J_{Coul}, which slightly surpasses J_{FB} in eq 4; the flat-band condition becomes, J_{Coul} = 1.19 J_{FB} = $\tilde{J}_{FB}$, where the tilde

DOI: 10.1021/acs.jpcc.9b04429
J. Phys. Chem. C 2019, 123, 20567−20578

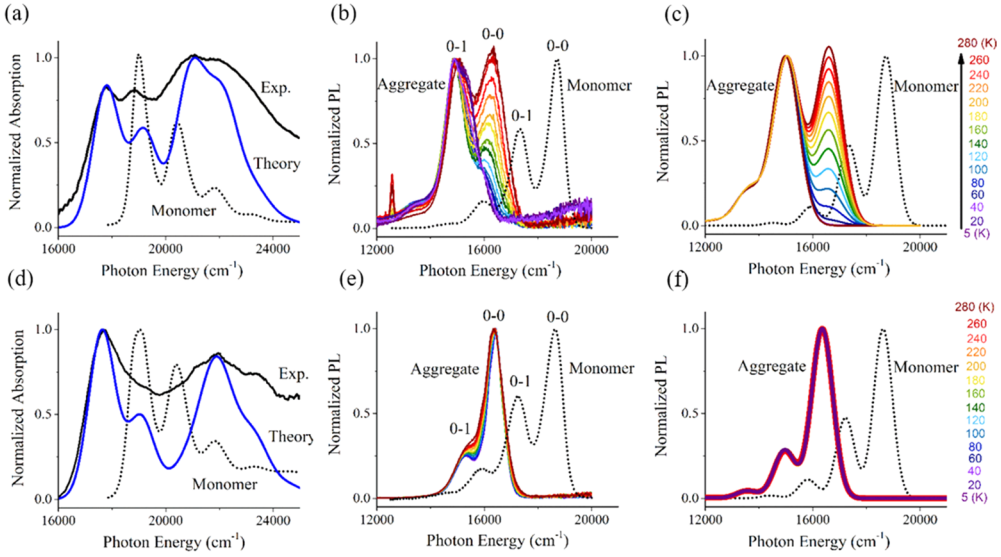

Figure 4. (a) Measured absorption spectrum for solution-phase (black dot) and crystalline (black solid) *N*-phenyl PDI. Theoretical spectrum for a 10-mer π-stack is shown in blue. (b) Measured temperature-dependent PL spectra for the crystalline and solution-phase forms of *N*-phenyl PDI normalized to the 0−1 peak intensity. (c) Calculated temperature-dependent PL spectra for *N*-phenyl PDI 10-mers. (d) Measured absorption spectrum for solution-phase (black dot) and crystalline (black solid) tetraphenyl PDI. The theoretical spectrum is shown in blue. (e) Measured temperature-dependent PL spectra for the crystalline and solution-phase forms of tetraphenyl PDI normalized to the 0−0 peak intensity. (f) Calculated temperature-dependent PL spectra for tetraphenyl PDI. The theoretical absorption and emission spectra in (a), (c), (d), and (f) were calculated using the Frenkel−CT/Holstein Hamiltonian in eq S.1 utilizing the Coulomb couplings in Table 1 and optimized parameters in Table S1 (including the relative dielectric constant).

overstrike indicates the inclusion of vibronic coupling. Increasing the Coulomb coupling beyond $\tilde{J}_{FB}$ causes band curvature inversion (the right panel of Figure 3), leading to the creation of an Hj-aggregate, where the H-promoting influence of the Coulomb coupling now outweighs the J-promoting influence of the Frenkel−CT exciton coupling.

Figure 3 also shows how the absorption and emission spectra of the vibronically coupled 10-mer π-stack respond to increasing J_{Coul} through the null point. The HR factor of unity ($\lambda^2 = 1$) allows one to more clearly appreciate the effect of intermolecular interactions on the vibronic progression: when $\lambda^2 = 1$, the first two vibronic peaks (0−0 and 0−1) in the monomer absorption (and PL) spectrum have equal intensity. For the 10-mer stack, the Figure portrays two broad, vibronically structured absorption peaks (A and B) resulting from the resonant Frenkel−CT exciton interactions. Such a two-band absorption structure has been observed in many PDI systems.[19,22−24,37,47,48] Using eq 3, the splitting (at $k = 0$) is approximately given by

$$\Delta_{AB} = 2\sqrt{2}|t_e + t_h| \quad (5)$$

as indicated by the double-headed arrow in the figure. Note the steady increase in the oscillator strength of the peak B with increasing Coulomb coupling due to the enhanced admixture of the optically bright $k = 0$ Frenkel exciton (the diabatic CT state is assumed to carry no oscillator strength). However, most important to what follows is the strong sensitivity of the temperature-dependent PL spectrum to the delicate balance between the two coupling influences. In hJ-aggregates (left lower panel), the emission is J-like with a dominant, superradiant 0−0 peak that diminishes with increasing temperature, whereas in Hj-aggregates (right panel), the emission is H-like with the weak 0−0 peak increasing steadily with temperature, as the $k = 0$ state—the sole source of 0−0 emission—is thermally activated.[29,35] Note that the null aggregate in the center panel is characterized by a monomer-like PL spectrum; for the monomer, the 0−0/0−1 ratio is equal to $1/\lambda^2$ (=1) and is temperature-independent.

Interestingly, the absorption spectral ratio a_1/a_2 in peak A does not provide the same clear signature of null-aggregate behavior as the PL spectral ratio does. In the flat-band limit (center panel), the ratio remains slightly larger than the monomer value, $1/\lambda^2$ (=1), as is also the case even for the Hj-aggregate in the right panel. As shown in ref 27, the entire absorption spectral line shape approaches that of the monomer in the limit that the diabatic CT and Frenkel bands become increasingly off-resonant (including the vanishing of band B). Hence, we rely instead on the temperature-dependent PL to determine aggregate nature and, in particular, the proximity to a null point.

Thus far, the model shows that by making subtle modifications to the aggregate structure, one can effect changes through a null point that have dramatic consequences for the photophysical properties of molecular aggregates. In what follows, we will show how the coupling between Frenkel and CT excitons in the presence of Coulomb coupling impacts the exciton band shape in both PDI derivatives, leading to the unusual hybrid (hJ and Hj) aggregate types.

III. EXPERIMENTAL ABSORPTION AND EMISSION SPECTRA

To validate our theoretical prediction of the switching between hJ and Hj behaviors, we have carried out absorption and photoluminescence (PL) spectroscopy in solution-grown tetraphenyl and *N*-phenyl PDI microcrystals. Sample preparation methods are detailed in the SI, along with optical microscopy and fluorescence microscopy images of the as-grown microcrystals (Figure S1). Figure 4 summarizes the steady-state absorption and PL spectra of the two derivatives in the solution and crystalline phases. The monomer absorption

DOI: 10.1021/acs.jpcc.9b04429
J. Phys. Chem. C 2019, 123, 20567−20578

spectra (Figure 4a,d, black dash) are very similar for the two derivatives: both monomers exhibit pronounced vibronic progressions in their absorption line shapes resembling most PDI families[14] resulting from coupling between the main $S_0 \rightarrow S_1$ electronic transition and the symmetric vinyl-stretching mode with frequency near 1400 cm^{-1} [49,50] and HR factor λ^2 = 0.6 (see Figure S5). The monomer PL spectrum closely mirrors that of the absorption spectrum.

Compared to monomeric solutions, the absorption spectrum of many PDI aggregates displays two asymmetrically broadened absorption bands with one red-shifted and the other blue-shifted relative to the main monomer peak.[19,22−24,37,47,48] A similar two-band structure is observed in tetraphenyl and *N*-phenyl PDI aggregates in Figure 4a,d, with the lowest energy electronic transition red-shifted by more than 1000 cm^{-1} relative to the monomer peak. As indicated in Figure 2, the long-range Coulomb coupling alone supports H-aggregates for both PDI derivatives and, therefore, blue-shifted absorption bands (compared to the monomer), entirely at odds with the reported spectra in Figure 4a,d. As we show here, the band splitting behavior observed in both PDI aggregates is primarily a result of the coupling between Frenkel and CT excitons in the resonant regime, driven by intermolecular electron and hole transfer, and not long-range Coulomb coupling. In general, however, both effects play an important role in determining the exciton band shape and the overall hybrid "HJ" nature of the photophysical response, as already indicated in Figure 3.

More clues to the H/J-behavior can be gathered from the temperature-dependent PL measurements. Figure 4b,e shows the steady-state PL spectra obtained from 5 to 280 K for the crystalline phases of both PDI derivatives. Measurements were performed on thin crystals to eliminate reabsorption effects, and all spectra were normalized to the dominant vibronic peak (the 0−1 peak in *N*-phenyl PDI and the 0−0 peak in tetraphenyl PDI). As can be appreciated from Figure 4b,e, the difference between the two PDI derivatives is striking: in the *N*-phenyl derivative, the 0−0 PL intensity (relative to the 0−1 intensity) almost vanishes at the lowest temperature but grows steadily with increasing temperature until it eventually surpasses the 0−1 peak. Such behavior is characteristic of weakly coupled H-aggregates where the 0−0 peak is thermally activated, as discussed in greater detail in the following section. By contrast, in the tetraphenyl derivative, the 0−0 peak remains dominant and several times larger than the 0−1 peak over the entire temperature range. The 0−0/0−1 intensity ratio is about twice that for the monomer, a strong indication of J-aggregation, but with a coherence limited to only a couple of chromophores, as the 0−0/0−1 ratio is approximately N_{coh} times greater than for the monomer in J-aggregates.[51,52] Here, N_{coh} is the number of coherently connected chromophores. In Section IV, we show that the temperature-stable ratio of approximately two is likely due to Peierls-like dimerization.

We further investigated the possible creation of excimers, which are quite common in PDIs,[53−59] by obtaining the time-resolved emission spectrum using a streak camera. Results are shown in the SI, where we demonstrate that, for tetraphenyl PDI, a slowly decaying red-shifted shoulder peak at ∼730 nm (Figure S2 in the SI) with <20% of the peak intensity of the main peak may be attributable to an excimer. This excimer spectral position is red-shifted from a previous report,[19] which suggested excimer-like emission at 675 nm from defect sites within a polycrystalline film of tetraphenyl PDI grown from physical vapor deposition but falls well within the reported range of 650−850 nm.[60] The discrepancy in the excimer emission could result from a different defect type due to different growth methods (solution-grown microcrystal in our case vs physical vapor deposited thin film in ref 19). Because the steady-state PL spectra are dominated by the exciton component and the ∼730 nm feature (13 600 cm^{-1}) is low enough in energy, the two main vibronic features present in Figure 5 should not be seriously impacted by the excimer. For *N*-phenyl PDI, no obvious excimer feature has been observed.

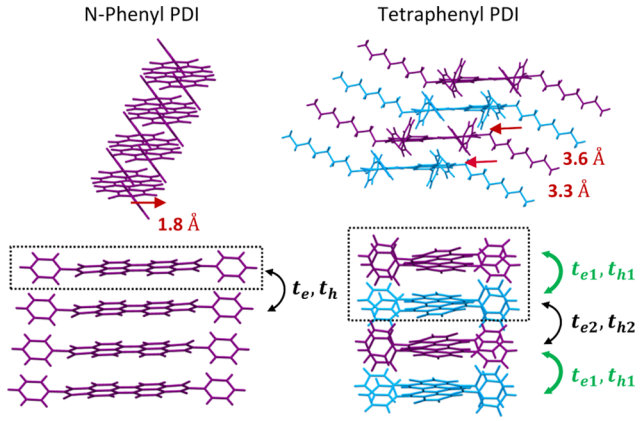

Figure 5. Several views of *N*-phenyl PDI (left) and tetraphenyl PDI (right) π-stacks taken from the known crystal structures, showing, respectively, slipping along the short-axis and long-axis. The two views of the tetraphenyl PDI π-stack show two molecules in a unit cell (related by inversion) giving rise to two sets of electron and hole transfer integrals. Note that the C8 tails have been removed in the bottom figure of tetraphenyl PDI for clarity.

The temperature dependence of the time-resolved PL lifetimes is also consistent with overall J- and H-like behaviors for tetraphenyl- and *N*-phenyl PDI aggregates, respectively. The experimental temperatures are varied from 5 to 280 K, and the experiments were conducted at low pump fluence to avoid exciton−exciton annihilation, as described in the SI. In the aggregate form, both PDIs display multiexponential PL decay dynamics. *N*-Phenyl PDI aggregates exhibit a 4-fold increase in the lifetime upon cooling to 5 K (τ_1 = 5.7 ns and τ_2 = 20.7 ns) in comparison to the lifetimes at 280 K (τ_1 = 1.6 ns and τ_2 = 5.1 ns), which could be attributed to the decreased population of the bright state at low temperature (Figure S3). In comparison, the PL lifetime of the tetraphenyl aggregates is several times shorter than *N*-phenyl PDI, possibly due to a faster-decaying (superradiant) radiative component. The lifetimes are also nearly temperature-independent between 40 and 280 K, suggesting a flat energy band, which we discuss further in Section IV.

In the following section we show how the disparate behaviors exhibited by the two PDI derivatives are consistent with the formation of hJ- and Hj-aggregates in tetraphenyl PDI and *N*-phenyl PDI, respectively.

IV. STRADDLING A NULL POINT: HJ-AGGREGATE BEHAVIOR IN *N*-PHENYL VS TETRAPHENYL PDI

In this section, we show how the packing details of the two PDI derivatives contribute to their opposing emission behaviors, i.e., their hJ and Hj behaviors. Figure 5 shows selected views of *N*-phenyl PDI and tetraphenyl PDI π-stacks,

DOI: 10.1021/acs.jpcc.9b04429
J. Phys. Chem. C 2019, 123, 20567−20578

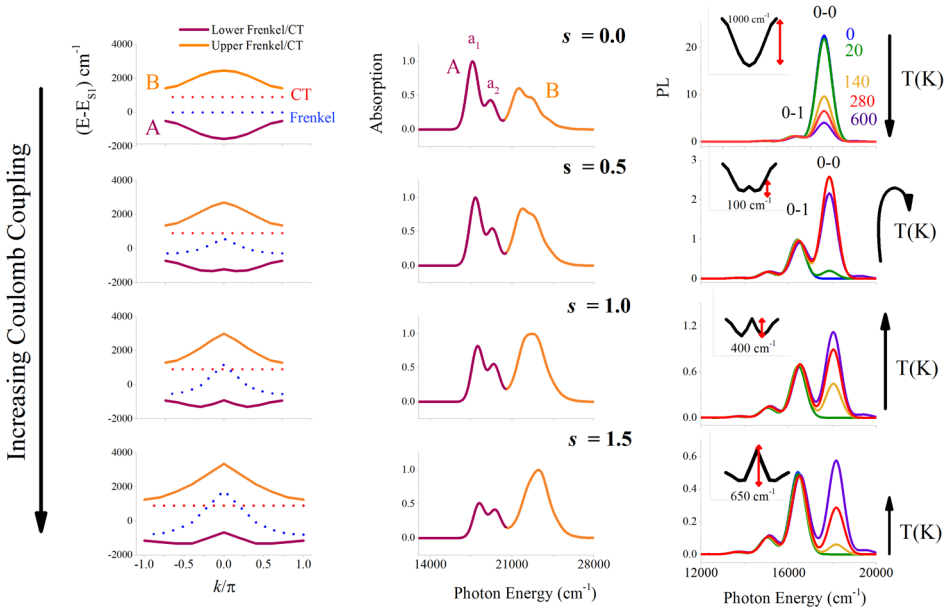

Figure 6. Calculated band dispersions (left), associated absorption spectrum (middle), and temperature-dependent PL spectra (right) for *N*-phenyl π-stacks as a function of increasing Coulombic coupling in going from top to bottom rows. The red (blue) dotted lines in the left panels are the diabatic CT (Frenkel) bands. Insets on the right panels show a magnified version of the band A dispersion indicating activation energy for 0−0 emission. Electronic coupling parameters are taken from Table 1 but with Coulomb couplings reduced by a factor of ε = 3 due to dielectric screening. The (screened) Coulombic couplings are multiplied by a scaling factor *s*, starting with *s* = 0 in the top row (no Coulomb coupling) and increasing to *s* = 1.5 in the bottom row. Band dispersions are evaluated without vibronic coupling. Spectral simulations were conducted on 10-mers, including vibronic coupling with ω_{vib} = 1400 cm^{-1} and λ^2 = 0.6, values which best fit the solution-phase spectrum in Figure 4, with anionic and cationic HR factors each equal to 0.3. $E_{CT} - E_{S_1}$ was set to 900 cm^{-1}. Spectra are evaluated using the Frenkel−CT/Holstein Hamiltonian, as described in the SI.

as determined from their known crystal structures. The n.n. separation in both cases is approximately 3.5 Å, but the relative orientations are quite different; in *N*-phenyl PDI, there is just one chromophore per unit cell (within a single π-stack) with the two n.n. chromophores shifted along the short molecular axis by approximately 1.8 Å. Conversely, tetraphenyl PDI has two molecules in a unit cell (within a π-stack), with neighbors displaced mainly along the long molecular axis by as much as 3.6 Å. The relative orientations are indicated in the contour plots of $-t_e t_h$ and J_{Coul} in Figure 2, which provides a qualitative assessment of the coupling interference. Interestingly, for both derivatives, the two CT integrals are in-phase, thereby supporting J-like short-range coupling, whereas the long-range coupling is positive and, therefore, H-promoting. The overall destructive interference leads to their hybrid HJ-aggregate nature, similar to what was found for TAT nanopillars.[26] As we will show, it is the competition between short- and long-range couplings, which is responsible for diverse emission behaviors observed for the two PDI derivatives.

In Table 1, we report results from more detailed calculations of the short-range and long-range couplings, which go beyond the perylene core approximation of Figure 2 and employ the full atomistic detail obtained from the X-ray diffraction data.[19,61] Care was taken to ensure a consistent phase assignment for transfer integrals and Coulomb integrals, as discussed in detail in the SI and ref 29. For *N*-phenyl PDI, the Coulomb couplings are uniformly positive and H-promoting, whereas the electron and hole transfer integrals, calculated via the method described in ref 62 are in-phase and J-promoting. Because there are two molecules in a unit cell for tetraphenyl PDI, there are two sets of electron and hole CT integrals labeled 1 and 2 in the Table. The former applies to the two molecules in a given unit cell, whereas set 2 applies to electron and hole transfer between two chromophores in neighboring unit cells. Hence, for tetraphenyl PDI, charge transfer differs to the "right" or "left" of a given chromophore. However, in both cases, t_e and t_h remain in-phase (J-promoting). The strong asymmetry in the short-range coupling leads to interesting dimer-like behavior, which results in band splitting, as explained in greater detail in the SI. The Coulomb couplings in tetraphenyl PDI are also divided into two sets, as shown in the table, to account for asymmetric couplings on each side of a chromophore; they remain dominantly positive (H-like), and, unlike in *N*-phenyl, are mostly confined to the nearest neighbors due to the very significant long-axis slip between neighboring molecules. The latter is also responsible for an eventual sign change in the coupling for chromophores beyond nearest neighbors.

In what follows, we analyze in detail the absorption and emission spectral line shapes for the two PDIs in turn, using the calculated values of t_e and t_h, the extended Coulomb couplings from Table 1 and the vibronic parameters deduced from the monomer absorption spectra in Figure 4a,d, see Figure S5. Spectral simulations are based on π-stacks containing 10 chromophores utilizing the Frenkel−CT/Holstein Hamiltonian, which treats vibronic coupling quantum mechanically. The Hamiltonian is represented in a two-particle basis set and numerically diagonalized to yield the eigenstates and eigenenergies, which are then used to construct the absorption and emission spectra. Details can be found in the SI.

IV.I. *N*-Phenyl PDI. To demonstrate the interference between short- and long-range couplings in *N*-phenyl PDI,

DOI: 10.1021/acs.jpcc.9b04429
J. Phys. Chem. C 2019, 123, 20567−20578

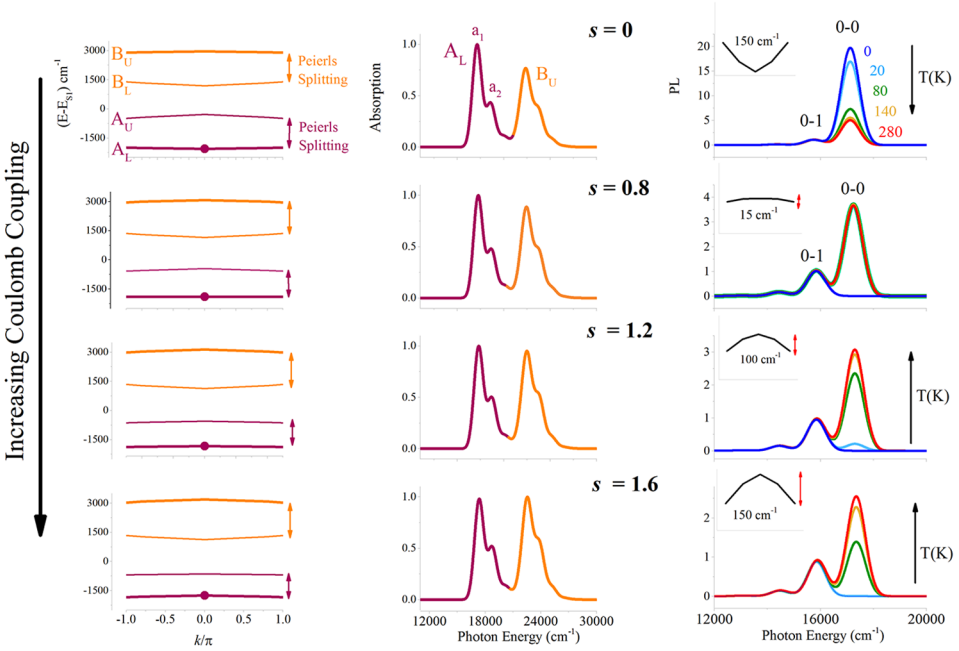

Figure 7. Calculated band dispersions (left), associated absorption spectrum (middle), and temperature-dependent PL spectra (right) for tetraphenyl PDI π-stacks as a function of increasing Coulombic coupling in going from top to bottom rows. Insets on the right panels show a magnified version of the band A dispersion indicating activation energy for 0−0 emission. Electronic coupling parameters are taken from Table 1 but with Coulomb couplings reduced by a factor of $\varepsilon = 3$ due to dielectric screening. The Coulombic couplings are multiplied by a scaling factor s, starting with $s = 0$ in the top row (no Coulomb coupling) and increasing to $s = 1.6$ in the bottom row. Band dispersions are evaluated without vibronic coupling. Spectral simulations were conducted on 10-mers including vibronic coupling with $\omega_{vib} = 1400$ cm^{-1} and $\lambda^2 = 0.6$, values which best fit the solution-phase spectrum in Figure 4, with anionic and cationic HR factors each equal to 0.3. $E_{CT} - E_{S_1}$ was set to 900 cm^{-1}. Spectra are evaluated using the Frenkel−CT/Holstein Hamiltonian, as described in the SI. The solid circle in the A_L band (left panels) indicates the bright $k = 0$ exciton, from which 0−0 emission derives. Note that the k values are referenced to an aggregate with two molecules per unit cell.

we show in Figure 6 the impact of increasing the Coulomb coupling on 10-mer π-stacks using the electronic couplings from Table 1 (the Coulomb couplings from the table were reduced by a factor of $\varepsilon = 3$ to account for dielectric screening). In Figure 6, the Coulomb coupling is increased in going from top to bottom, whereas the CT integrals remain constant; all of the screened Coulomb couplings from Table 1 are scaled by a factor, s, beginning with $s = 0$ (top), i.e., no Coulomb coupling, and increasing in even increments to $s = 1.5$ (bottom). In addition, we take the diabatic CT band to be offset by, $E_{CT} - E_{S_1} = 1000$ cm^{-1}, a reasonable value in agreement with previous works.[26] We note that since $|t_e + t_h|$ remains much greater than the offset, we are well within the (near) resonance regime of Frenkel−CT coupling.

As observed from the panels in the topmost row, in the limit of no Coulombic coupling, the dispersionless, diabatic Frenkel, and CT exciton bands interact to create bands A and B with maximum splitting at $k = 0$, as follows from the in-phase relationship between t_e and t_h. Hence, a $k = 0$ exciton resides at the bottom of band A, as defines J-aggregates. Based on the values of t_e and t_h for N-phenyl (see Table 1), the predicted band splitting from eq 5 is

$$\Delta_{AB} = 2\sqrt{2}\,|t_e + t_h| \approx 4000 \text{ cm}^{-1}$$

in good agreement with the actual splitting in the presence of vibronic coupling, as determined from the absorption spectrum (middle panel). The large splitting is responsible for a substantial red-shift of peak A by about 1000 cm^{-1} from the monomer peak (at approximately 19 000 cm^{-1}). Moreover, the ratio of the vibronic intensities a_1/a_2 is noticeably larger than the monomer value of approximately $1/\lambda^2 = 1.67$, as is characteristic of J-aggregates.[35] Also, note the significant asymmetry between peaks A and B. The greater oscillator strength in peak A is due mainly to the ordering of the diabatic Frenkel and CT bands. Since the Frenkel band is lower in energy, the band A excitons have slightly more Frenkel character, giving peak A slightly more oscillator strength (the diabatic CT excitons are assumed to carry no oscillator strength). Turning to the PL spectrum, we again see clear J-like behavior: the 0−0 component is dominant, with the 0−0/0−1 ratio exceeding the monomer ratio by about a factor of N (=10) at very low temperatures.[51] The ratio decreases with the increasing temperature, as the $k = 0$ exciton, the only one which can source 0−0 emission, is thermally depleted.[35,51]

Increasing the Coulomb coupling to half-strength (second row in Figure 6) already shows evidence of the destructive interference between the two coupling sources. The positive Coulombic couplings result in a diabatic ("before-mixing") Frenkel band shown in blue with negative curvature, i.e., the $k = 0$ Frenkel exciton is on top of the band, as defines Kasha H-aggregates. However, subsequent mixing with the dispersionless CT band (in red) produces an unusual mustache-shaped dispersion for band A,[26] in which the $k = 0$ exciton now lies within the band, approximately 100 cm^{-1} above the band bottom. The intermediate position of the $k = 0$ exciton is a hallmark characteristic of the destructive interference inherent to HJ-aggregates[29] and follows from eq 3 when using extended Coulomb interactions. Thermal activation is now required to populate the $k = 0$ exciton to provide 0−0 emission. The PL spectrum, therefore, shows hybrid HJ behavior, an initial H-

DOI: 10.1021/acs.jpcc.9b04429
J. Phys. Chem. C 2019, 123, 20567−20578

like growth with increasing temperature, which eventually rolls over and undergoes a J-like decay with further temperature increases.[63] Finally, note that the A−B band splitting in the absorption spectrum hardly changes with the increase in Coulomb coupling to s = 0.5, since the splitting is mainly sensitive to the sum $|t_e + t_h|$. Peak B does, however, acquire greater oscillator strength compared to the case when Coulomb coupling is absent (top row) due to the enhanced resonance between the k = 0 diabatic CT and Frenkel excitons observed in the left panel.

Further increasing the Coulomb coupling (last two rows in Figure 6) results in a continued increase in peak B intensity so that it becomes the dominant band. The increased Coulomb coupling also results in a diminishing a_1/a_2 ratio as the H-character continues to increase, for example, when s = 1.5 (last row) a_1/a_2 is approximately 1.2, substantially less than the monomer value of $1/\lambda^2$ = 1.67. Moreover, the increased activation energy for populating the k = 0 exciton within the mustache-shaped dispersion band leads to a monotonic H-like increase in the 0−0 peak relative to the 0−1 peak in the PL spectrum with no roll-over to J-like behavior as is observed when s = 0.5. Note that when s = 1 the spectral characteristics are qualitatively very similar to what was obtained experimentally for *N*-phenyl, see Figure 4c. When we fine-tune the couplings for optimal agreement between the simulated and measured spectra (as described in the caption of Figure 4) we obtain the spectra shown in Figure 4a,c, which agree well with experiment.

IV.II. Tetraphenyl PDI. As reported in Table 1, in tetraphenyl PDI π-stacks, the n.n. Coulomb coupling is positive (H-promoting) but rapidly decreases (and even becomes negative) for more distant neighbors due to the significant longitudinal shift between neighboring chromophores. The short-range coupling is J-promoting (t_e and t_h are in-phase) but is strongly asymmetric due to the slightly different shifts experienced by the right and left nearest neighbors (see Figure 5) and the extreme sensitivity of both electron and hole transfer integrals to sub-angstrom shifts in geometry, see Figures 2 and 5. The calculated electron and hole transfer integrals are largest between the two chromophores in a unit cell (t_{e1}, t_{h1}) and much weaker between chromophores in different (but neighboring) unit cells (t_{e2}, t_{h2}). In what follows it is convenient to view the π-stack as a linear array of coupled dimers, where each dimer is comprised of the two strongly coupled molecules within a unit cell.

To understand how the asymmetry in the short-range coupling affects the exciton band structure, we first examine the simplest case where there is no Coulomb coupling (row 1 in Figure 7). The strong asymmetry in the CT transfer integrals create a Peierls-like band splitting within both the lower and upper adiabatic Frenkel−CT bands, leading to the creation of the lower-energy bands A_L and A_U as well as the higher-energy bands B_L and B_U as demonstrated in the left panel of Figure 7. The A band (and B band) splitting depends mainly on the interference between the short-range coupling induced by the large intradimer transfer integrals (compared to the interdimer transfer integrals) and the intradimer Coulomb coupling. The case in which t_e and t_h are in-phase, as occurs in tetraphenyl PDI, the short-range coupling is J-promoting, so that when J_{Coul} = 0, oscillator strength is deposited in the lowest energy state, the k = 0 exciton in the band A_L, with the band A_U remaining optically dark to absorption. By contrast, in the higher-energy band, the oscillator strength is consumed by the k = 0 exciton in B_U (B_L is optically dark). Hence, the absorption spectrum retains the two-band structure with a red-shifted peak A_L accompanied by a blue-shifted peak B_U, with a band splitting $\Delta_{A_LB_U}$ of about 4600 cm^{-1} from Figure 7 (top middle panel). The splitting agrees well with the exact expression derived for two molecules per unit cell in the absence of vibronic coupling

$$\Delta_{A_LB_U} = 2\sqrt{(t_{e1} + t_{h1})^2 + (t_{e2} + t_{h2})^2} \quad (6)$$

Note that eq 6 reduces to eq 5 when there is no asymmetry ($t_{e1} = t_{e2}$ and $t_{h1} = t_{h2}$).

The temperature dependence of the PL spectrum ultimately arises from the shape of the lower band A_L, which, in the absence of Coulomb coupling, maintains a positive curvature (J-like) with the bright k = 0 state at the band minimum. Hence, as observed in Figure 7 (top right panel), the emission is J-like, with the 0−0/0−1 PL ratio significantly larger than that of the monomer at low temperatures but decreasing significantly with increasing temperature (as the bright k = 0 population is depleted). Note that even at the highest temperature, the 0−0/0−1 PL ratio is about twice the monomer value, as in a J-dimer (see the SI), because k_bT is still much smaller than the A_L−A_U band splitting.

As the Coulomb coupling increases, the two-band absorption spectrum in Figure 7 is almost an invariant. Here, the H-like Coulomb coupling is not strong enough, even at its highest setting (s = 1.6), to significantly alter the large intradimer splitting between the A_L and A_U bands induced by the short-range interactions. Therefore, the intradimer interactions remain dominantly J-like in all cases, where the lowest energy band (A_L) possesses the bright k = 0 state. However, the Coulomb coupling does eventually invert the curvature of the (emitting) A_L band, since it can more easily destructively interfere with the weaker interdimer short-range couplings. This is reflected in the temperature dependence of the PL spectra: when the A_L band is almost completely rendered flat (s = 0.8), the PL line shape is practically temperature-independent resembling that of a J-dimer at all temperatures, i.e., what one would expect from a system of uncoupled dimers. For larger Coulomb couplings, the A_L band curvature becomes negative, and the PL spectrum becomes H-like with the 0−0/0−1 peak ratio now increasing with temperature. Note that at the highest temperatures, for all Coulomb couplings considered in Figure 7, any small curvature in the lower band is overcome by k_bT, and the PL spectrum evolves into the J-dimer line shape, where the 0−0/0−1 ratio is about twice that of the monomer.

The experimental PL spectrum of tetraphenyl PDI in Figure 4e exhibits almost no temperature dependence of the 0−0/0−1 ratio, with a 0−0/0−1 ratio about twice as large the monomer, consistent with a positive (H-promoting) Coulomb coupling, which is strong enough to nullify the interdimer short-range coupling, resulting in emission akin to non-interacting J-dimers. Hence, tetraphenyl PDI forms hJ-aggregates. When we fine tune the couplings (as reported in the caption of Figure 4) for optimal agreement between the simulated and measured spectra, we obtain the spectra shown in Figure 4d,f. The simulated absorption spectrum agrees well with the experiment and manages to account for the vibronic structure spread over the two main (A, B) peaks. Interestingly, as for *N*-phenyl PDI, the electron and hole integrals require a scaling by 0.8 to accurately reproduce the A/B splitting. Most

DOI: 10.1021/acs.jpcc.9b04429
J. Phys. Chem. C 2019, 123, 20567−20578

importantly, the temperature independence and shape of the PL spectrum agree well with the experiment.

V. DISCUSSION/CONCLUSIONS

We measured the steady-state absorption and emission spectra of the solution (unaggregated) and crystal phases of two PDI derivatives, *N*,*N*′-bis(*n*-octyl)-2,5,8,11-tetraphenyl PDI and *N*,*N*′-bis(phenyl)-PDI, and analyzed the spectral line shapes theoretically using the Frenkel−CT/Holstein Hamiltonian. Both derivatives show convincing evidence of an effective destructive interference between the H-promoting Coulomb couplings and the J-promoting short-range couplings derived from intermolecular charge transfer between neighboring chromophores within a π-stack. Interestingly, the two derivatives straddle a null point, the point at which the destructive interference is so efficient as to create a flat dispersionless exciton band, but appear on opposite sides, as determined primarily by the temperature-dependent steady-state PL line shapes. Hence, *N*-phenyl PDI, with slightly dominant Coulomb interactions, forms Hj-aggregates, whereas tetraphenyl PDI with slightly dominant short-range interactions, forms a chain of hJ-dimers.

Both PDI derivatives produce similar absorption spectra in the crystal phase, characterized by two main bands, A and B. The band splitting is reflective of strong resonant coupling between the $k = 0$ Frenkel and CT excitons, driven by the in-phase electron and hole transfer integrals ($t_e t_h > 0$). The stronger Coulomb coupling in *N*-phenyl PDI leads to a slightly larger oscillator strength in the higher-energy band (B) versus the lower-energy band (A), whereas in the more J-like tetraphenyl PDI, the oscillator strength is larger in the band (A). However, a far more dramatic difference exists in the PL spectra. *N*-Phenyl PDI displays classic H-like emission behavior,[35] with the 0−0/0−1 PL ratio increasing monotonically with increasing temperature, whereas tetraphenyl PDI displays a J-like PL spectrum with a dominant 0−0 peak. In tetraphenyl PDI, the 0−0/0−1 ratio exceeds the monomer value by about a factor of 2 and is practically independent of temperature, indicative of dimer localization caused by the presence of two strongly coupled molecules per unit cell. The opposing PL spectral behaviors best reflect the competition between the H-promoting Coulomb coupling and the J-promoting CT-mediated coupling. In *N*-phenyl PDI π-stacks the larger Coulomb coupling, arising from the more efficient (side-by-side) overlap between neighboring chromophores, tilts the scales in favor of H-like PL behavior (Hj-aggregates). Conversely, in the hJ-aggregates (π-stacks) of tetraphenyl PDI, neighboring chromophores are longitudinally displaced by more than 3 Å, leading to a much weaker (but still positive and, therefore, H-promoting) Coulomb coupling, which is overwhelmed by the stronger J-promoting CT-mediated coupling within the unit cell "dimers".

Despite the overall good agreement between the calculated and measured spectra, there remain some notable discrepancies. For example, in the PL spectrum for *N*-phenyl PDI, the 0−0 peak retains a small but significant intensity down to the lowest temperatures, ≈5 K. This is very likely the result of static disorder in the form of site imperfections, such as vacancies, chemical impurities, and localized stress, or, from longer-range structural imperfections, such as stacking faults and dislocations.[64] Such defects have been studied theoretically in oligoacenes[65] as well as oligothiophene and oligophenylene−vinylene herringbone lattices[66−68] but have not been included in the present work. Disorder breaks the translational symmetry, causing the band states to mix. As a result, the lowest energy (emitting) state, which is a $k \neq 0$ exciton in *N*-phenyl PDI, borrows 0−0 oscillator strength from the bright $k = 0$ state, which exists at slightly higher energies (see the exciton band shapes in Figure 6). Energy transfer within a disordered landscape also enhances the Stokes shift; in both PDI derivatives, the Stokes shift is larger in the solid phase (1200−1400 cm^{-1}) versus the solution (300−400 cm^{-1}). In future work, we will test these hypotheses by averaging over disorder ensembles with varying degrees of spatial correlation.

Future work will also focus on exciton dynamics in the Hj versus hJ PDI systems. We expect that dimer trapping in tetraphenyl PDI will lead to a diminished diffusion constant for exciton transport along the π-stacking direction. Such trapping and subsequent ultrafast, intradimer relaxation has been suggested in several works.[69−71] We also plan to evaluate exciton−exciton annihilation in both PDI derivatives, hoping to reveal further differences due to the destructive relationship between short- and long-range couplings. The proximity to a null point means that relatively small perturbations, such as the application of hydrostatic pressure or chemical tuning, can cause hJ and Hj interconversions as revealed through changes in temperature-dependent PL line shapes and possibly changes in exciton diffusion coefficients. The ability to direct such changes would represent a significant step in furthering our goal of band shape engineering for targeted applications.

■ ASSOCIATED CONTENT

Supporting Information

The Supporting Information is available free of charge on the ACS Publications website at DOI: 10.1021/acs.jpcc.9b04429.

Sample preparation and details of the optical measurements, the Frenkel−CT Hamiltonian and its parameterization, expressions for the absorption and emission spectra, dimer analysis and an in-depth discussion of the phase convention for the intermolecular interactions (PDF)

■ AUTHOR INFORMATION

Corresponding Author

*E-mail: spano@temple.edu.

ORCID

Mingji Dai: 0000-0001-7956-6426
Roel Tempelaar: 0000-0003-0786-7304
Libai Huang: 0000-0001-9975-3624
Frank C. Spano: 0000-0003-3044-6727

Author Contributions

⊥A.O. and T.Z. contributed equally to this work.

Notes

The authors declare no competing financial interest.

■ ACKNOWLEDGMENTS

This work was carried out with the financial support for F.C.S. from the National Science Foundation (DMR-1810838). The experimental work at Purdue is supported by U.S. National Science Foundation (NSF) through grant NSF-CHE-1555005. I.S.D. acknowledges support from the United States Department of Energy through the Computational Sciences Graduate Fellowship (DOE CSGF) under grant number: DE-FG02-97ER25308. D.R.R. acknowledges funding from NSF Grant

DOI: 10.1021/acs.jpcc.9b04429
J. Phys. Chem. C 2019, 123, 20567−20578

No. CHE-1839464. D.B. thanks the Deutsche Forschungsgemeinschaft (DFG, German Research Foundation) for a research fellowship (project number 398287490). We thank Dr. Gary Wiederrecht, Dr. Richard Schaller, and Alexandra Brumberg at the Center for Nanoscale Materials at Argonne National Laboratory for their assistance with the streak camera measurements and Dr. Martina Lessio and Benedikt Kloss for helpful discussion regarding the Coulomb coupling calculations.

REFERENCES

(1) Heeger, A. J. Semiconducting Polymers: The Third Generation. *Chem. Soc. Rev.* **2010**, *39*, 2354−2371.
(2) Forrest, S. R. The Path to Ubiquitous and Low-Cost Organic Electronic Appliances on Plastic. *Nature* **2004**, *428*, 911−918.
(3) Friend, R. H.; Gymer, R. W.; Holmes, A. B.; Burroughes, J. H.; Marks, R. N.; Taliani, C.; Bradley, D. D. C.; Santos, D. A. D.; Brédas, J. L.; Logdlund, M.; et al. Electroluminescence in Conjugated Polymers. *Nature* **1999**, *397*, 121−128.
(4) Sirringhaus, H.; Tessler, N.; Friend, R. H. Integrated Optoelectronic Devices Based on Conjugated Polymers. *Science* **1998**, *280*, 1741−1744.
(5) Burroughes, J. H.; Bradley, D. D. C.; Brown, A. R.; Marks, R. N.; Mackay, K.; Friend, R. H.; Burns, P. L.; Holmes, A. B. Light-Emitting Diodes Based on Conjugated Polymers. *Nature* **1990**, *347*, 539−541.
(6) Brabec, C. J. Organic Photovoltaics: Technology and Market. *Sol. Energy Mater. Sol. Cells* **2004**, *83*, 273−292.
(7) Bao, Z. Materials and Fabrication Needs for Low-Cost Organic Transistor Circuits. *Adv. Mater.* **2000**, *12*, 227−230.
(8) Henson, Z. B.; Müllen, K.; Bazan, G. C. Design Strategies for Organic Semiconductors Beyond the Molecular Formula. *Nat. Chem.* **2012**, *4*, 699.
(9) McRae, E. G.; Kasha, M. Enhancement of Phosphorescence Ability Upon Aggregation of Dye Molecules. *J. Chem. Phys.* **1958**, *28*, 721−722.
(10) Kasha, M. Energy Transfer Mechanisms and the Molecular Exciton Model for Molecular Aggregates. *Radiat. Res.* **1963**, *20*, 55−70.
(11) Kasha, M.; Rawls, H. R.; El-Bayoumi, M. A. *The Exciton Model in Molecular Spectroscopy*; Butterworths: London, 1965; Vol. *11*.
(12) Chen, L.; Li, C.; Müllen, K. Beyond Perylene Diimides: Synthesis, Assembly and Function of Higher Rylene Chromophores. *J. Mater. Chem. C* **2014**, *2*, 1938−1956.
(13) Zhan, X.; Facchetti, A.; Barlow, S.; Marks, T. J.; Ratner, M. A.; Wasielewski, M. R.; Marder, S. R. Rylene and Related Diimides for Organic Electronics. *Adv. Mater.* **2011**, *23*, 268−284.
(14) Würthner, F.; Saha-Möller, C. R.; Fimmel, B.; Ogi, S.; Leowanawat, P.; Schmidt, D. Perylene Bisimide Dye Assemblies as Archetype Functional Supramolecular Materials. *Chem. Rev.* **2016**, *116*, 962−1052.
(15) Würthner, F. Perylene Bisimide Dyes as Versatile Building Blocks for Functional Supramolecular Architectures. *Chem. Commun.* **2004**, 1564−1579.
(16) Wilson, T. M.; Tauber, M. J.; Wasielewski, M. R. Toward an N-Type Molecular Wire: Electron Hopping within Linearly Linked Perylenediimide Oligomers. *J. Am. Chem. Soc.* **2009**, *131*, 8952−8957.
(17) Jones, B. A.; Facchetti, A.; Wasielewski, M. R.; Marks, T. J. Tuning Orbital Energetics in Arylene Diimide Semiconductors. Materials Design for Ambient Stability of N-Type Charge Transport. *J. Am. Chem. Soc.* **2007**, *129*, 15259−15278.
(18) Würthner, F.; Stolte, M. Naphthalene and Perylene Diimides for Organic Transistors. *Chem. Commun.* **2011**, *47*, 5109−5115.
(19) Eaton, S. W.; Shoer, L. E.; Karlen, S. D.; Dyar, S. M.; Margulies, E. A.; Veldkamp, B. S.; Ramanan, C.; Hartzler, D. A.; Savikhin, S.; Marks, T. J.; et al. Singlet Exciton Fission in Polycrystalline Thin Films of a Slip-Stacked Perylenediimide. *J. Am. Chem. Soc.* **2013**, *135*, 14701−14712.
(20) Le, A. K.; Bender, J. A.; Arias, D. H.; Cotton, D. E.; Johnson, J. C.; Roberts, S. T. Singlet Fission Involves an Interplay between Energetic Driving Force and Electronic Coupling in Perylenediimide Films. *J. Am. Chem. Soc.* **2018**, *140*, 814−826.
(21) Le, A. K.; Bender, J. A.; Roberts, S. T. Slow Singlet Fission Observed in a Polycrystalline Perylenediimide Thin Film. *J. Phys. Chem. Lett.* **2016**, *7*, 4922−4928.
(22) Ghosh, S.; Li, X.-Q.; Stepanenko, V.; Würthner, F. Control of H- and J-Type P Stacking by Peripheral Alkyl Chains and Self-Sorting Phenomena in Perylene Bisimide Homo- and Heteroaggregates. *Chem. − Eur. J.* **2008**, *14*, 11343−11357.
(23) Yagai, S.; Seki, T.; Karatsu, T.; Kitamura, A.; Würthner, F. Transformation from H- to J-Aggregated Perylene Bisimide Dyes by Complexation with Cyanurates. *Angew. Chem., Int. Ed.* **2008**, *47*, 3367−3371.
(24) Sarbu, A.; Biniek, L.; Guenet, J.-M.; Mesini, P. J.; Brinkmann, M. Reversible J- to H-Aggregate Transformation in Thin Films of a Perylenebisimide Organogelator. *J. Mater. Chem. C* **2015**, *3*, 1235−1242.
(25) Hestand, N. J.; Spano, F. C. Molecular Aggregate Photophysics Beyond the Kasha Model: Novel Design Principles for Organic Materials. *Acc. Chem. Res.* **2017**, *50*, 341−350.
(26) Yamagata, H.; Maxwell, D. S.; Fan, J.; Kittilstved, K. R.; Briseno, A. L.; Barnes, M. D.; Spano, F. C. Hj-Aggregate Behavior of Crystalline 7,8,15,16-Tetraazaterrylene: Introducing a New Design Paradigm for Organic Materials. *J. Phys. Chem. C* **2014**, *118*, 28842−28854.
(27) Hestand, N. J.; Spano, F. C. Interference between Coulombic and Ct-Mediated Couplings in Molecular Aggregates: H- to J-Aggregate Transformation in Perylene-Based Pi-Stacks. *J. Chem. Phys.* **2015**, *143*, No. 244707.
(28) Hestand, N. J.; Tempelaar, R.; Knoester, J.; Jansen, T. L. C.; Spano, F. C. Exciton Mobility Control through Sub-Angstrom Packing Modifications in Molecular Crystals. *Phys. Rev. B* **2015**, *91*, No. 195315.
(29) Hestand, N. J.; Spano, F. C. Expanded Theory of H- and J-Molecular Aggregates: The Effects of Vibronic Coupling and Intermolecular Charge Transfer. *Chem. Rev.* **2018**, *118*, 7069−7163.
(30) Tempelaar, R.; Jansen, T. L. C.; Knoester, J. Exciton−Exciton Annihilation Is Coherently Suppressed in H-Aggregates, but Not in J-Aggregates. *J. Phys. Chem. Lett.* **2017**, *8*, 6113−6117.
(31) Marques, S. R.; Labastide, J. A.; Barnes, M. D. Evolution of Hj Coupling in Nanoscale Molecular Self-Assemblies. *J. Phys. Chem. C* **2018**, *122*, 15723−15728.
(32) Wang, P.; Barnes, M. D. Disentangling "Bright" and "Dark" Interactions in Ordered Assemblies of Organic Semiconductors. *Nano Lett.* **2017**, *17*, 6949−6953.
(33) Kaufmann, C.; Bialas, D.; Stolte, M.; Würthner, F. Discrete Π-Stacks of Perylene Bisimide Dyes within Folda-Dimers: Insight into Long- and Short-Range Exciton Coupling. *J. Am. Chem. Soc.* **2018**, *140*, 9986−9995.
(34) Spano, F. C. Analysis of the UV/Vis and Cd Spectral Line Shapes of Carotenoid Assemblies: Spectral Signatures of Chiral H-Aggregates. *J. Am. Chem. Soc.* **2009**, *131*, 4267−4278.
(35) Spano, F. C. The Spectral Signatures of Frenkel Polarons in H- and J-Aggregates. *Acc. Chem. Res.* **2010**, *43*, 429−439.
(36) Gisslén, L.; Scholz, R. Crystallochromy of Perylene Pigments: Influence of an Enlarged Polyaromatic Core Region. *Phys. Rev. B* **2011**, *83*, No. 155311.
(37) Gisslén, L.; Scholz, R. Crystallochromy of Perylene Pigments: Interference between Frenkel Excitons and Charge-Transfer States. *Phys. Rev. B* **2009**, *80*, No. 115309.
(38) Hoffmann, M.; Soos, Z. G. Optical Absorption Spectra of the Holstein Molecular Crystal for Weak and Intermediate Electronic Coupling. *Phys. Rev. B* **2002**, *66*, No. 024305.
(39) Hoffmann, M.; Schmidt, K.; Fritz, T.; Hasche, T.; Agranovich, V. M.; Leo, K. The Lowest Energy Frenkel and Charge-Transfer Excitons in Quasi-One-Dimensional Structures: Application to MePTCDI and PTCDA Crystals. *Chem. Phys.* **2000**, *258*, 73−96.

DOI: 10.1021/acs.jpcc.9b04429
J. Phys. Chem. C 2019, 123, 20567−20578

(40) Merrifield, R. E. Ionized States in a One-Dimensional Molecular Crystal. *J. Chem. Phys.* **1961**, *34*, 1835−1839.
(41) Chang, J. C. Monopole Effects on Electronic Excitation Interactions between Large Molecules. I. Application to Energy Transfer in Chlorophylls. *J. Chem. Phys.* **1999**, *67*, 3901−3909.
(42) Beljonne, D.; Pourtois, G.; Silva, C.; Hennebicq, E.; Herz, L. M.; Friend, R. H.; Scholes, G. D.; Setayesh, S.; Müllen, K.; Brédas, J. L. Interchain Vs. Intrachain Energy Transfer in Acceptor-Capped Conjugated Polymers. *Proc. Natl. Acad. Sci. U.S.A.* **2002**, *99*, 10982−10987.
(43) Yamagata, H.; Pochas, C. M.; Spano, F. C. Designing J- and H-Aggregates through Wave Function Overlap Engineering: Applications to Poly(3-Hexylthiophene). *J. Phys. Chem. B* **2012**, *116*, 14494−14503.
(44) Note that the energy scale for the contour plot of the Coulombic coupling in Figure 2 has been corrected from ref 25. The *unscreened* Coulomb coupling between two perfectly eclipsed perylenes separated by 0.35 nm is about 1000 wavenumbers. (In Figure 4f of ref 25 the eclipsed value is approximately 350 wave numbers because the Coulomb couplings, although reported as unscreened, were actually scaled by a factor of $1/\varepsilon$, with the relative dielectric constant, $\varepsilon = 3$.)
(45) There is also a third band of degenerate CT excitons with energy E_{CT} which do not couple to the Frenkel excitons and hence carry no oscillator strength, see ref 25.
(46) Kasha, M. Characterization of Electronic Transitions in Complex Molecules. *Discuss. Faraday Soc.* **1950**, *9*, 14−19.
(47) Mizuguchi, J.; Tojo, K. Electronic Structure of Perylene Pigments as Viewed from the Crystal Structure and Excitonic Interactions. *J. Phys. Chem. B* **2002**, *106*, 767−772.
(48) Hartnett, P. E.; Timalsina, A.; Matte, H. S. S. R.; Zhou, N.; Guo, X.; Zhao, W.; Facchetti, A.; Chang, R. P. H.; Hersam, M. C.; Wasielewski, M. R.; et al. Slip-Stacked Perylenediimides as an Alternative Strategy for High Efficiency Nonfullerene Acceptors in Organic Photovoltaics. *J. Am. Chem. Soc.* **2014**, *136*, 16345−16356.
(49) Scholz, R.; Schreiber, M. Linear Optical Properties of Perylene-Based Chromophores. *Chem. Phys.* **2006**, *325*, 9−21.
(50) Heinemeyer, U.; Scholz, R.; Gisslén, L.; Alonso, M. I.; Osso, J. O.; Garriga, M.; Hinderhofer, A.; Kytka, M.; Kowarik, S.; Gerlach, A.; et al. Exciton-Phonon Coupling in Diindenoperylene Thin Films. *Phys. Rev. B* **2008**, *78*, No. 085210.
(51) Spano, F. C.; Yamagata, H. Vibronic Coupling in J-Aggregates and Beyond: A Direct Means of Determining the Exciton Coherence Length from the Photoluminescence Spectrum. *J. Phys. Chem. B* **2011**, *115*, 5133−5143.
(52) Hestand, N. J.; Spano, F. C. Determining the Spatial Coherence of Excitons from the Photoluminescence Spectrum in Charge-Transfer J-Aggregates. *Chem. Phys.* **2016**, *481*, 262−271.
(53) De Witte, P. A. J.; Hernando, J.; Neuteboom, E. E.; van Dijk, E. M. H. P.; Meskers, S. C. J.; Janssen, R. A. J.; van Hulst, N. F.; Nolte, R. J. M.; García-Parajó, M. F.; Rowan, A. E. Synthesis and Characterization of Long Perylenediimide Polymer Fibers: From Bulk to the Single-Molecule Level. *J. Phys. Chem. B* **2006**, *110*, 7803−7812.
(54) Son, M.; Park, K. H.; Shao, C.; Würthner, F.; Kim, D. Spectroscopic Demonstration of Exciton Dynamics and Excimer Formation in a Sterically Controlled Perylene Bisimide Dimer Aggregate. *J. Phys. Chem. Lett.* **2014**, *5*, 3601−3607.
(55) Chen, Z.; Stepanenko, V.; Dehm, V.; Prins, P.; Siebbeles, L. D. A.; Seibt, J.; Marquetand, P.; Engel, V.; Würthner, F. Photoluminescence and Conductivity of Self-Assembled Π−Π Stacks of Perylene Bisimide Dyes. *Chem. − Eur. J.* **2007**, *13*, 436−449.
(56) Langhals, H.; Ismael, R. Cyclophanes as Model Compounds for Permanent, Dynamic Aggregates − Induced Chirality with Strong Cd Effects. *Eur. J. Org. Chem.* **1998**, *1998*, 1915−1917.
(57) Chen, Y.; Kong, Y.; Wang, Y.; Ma, P.; Bao, M.; Li, X. Supramolecular Self-Assembly Study of a Flexible Perylenetetracarboxylic Diimide Dimer in Langmuir and Langmuir−Blodgett Films. *J. Colloid Interface Sci.* **2009**, *330*, 421−427.
(58) Son, M.; Fimmel, B.; Dehm, V.; Würthner, F.; Kim, D. Folding-Induced Modulation of Excited-State Dynamics in an Oligophenylene−Ethynylene-Tethered Spiral Perylene Bisimide Aggregate. *ChemPhysChem* **2015**, *16*, 1757−1767.
(59) Lim, J. M.; Kim, P.; Yoon, M. C.; Sung, J.; Dehm, V.; Chen, Z. J.; Würthner, F.; Kim, D. Exciton Delocalization and Dynamics in Helical Pi-Stacks of Self-Assembled Perylene Bisimides. *Chem. Sci.* **2013**, *4*, 388−397.
(60) Kennehan, E. R.; Grieco, C.; Brigeman, A. N.; Doucette, G. S.; Rimshaw, A.; Bisgaier, K.; Giebink, N. C.; Asbury, J. B. Using Molecular Vibrations to Probe Exciton Delocalization in Films of Perylene Diimides with Ultrafast Mid-Ir Spectroscopy. *Phys. Chem. Chem. Phys.* **2017**, *19*, 24829−24839.
(61) Sato, K.; Mizuguchi, J. *CCDC 628382: Experimental Crystal Structure Determination*; Cambridge Crystallographic Data Centre, 2007.
(62) Valeev, E. F.; Coropceanu, V.; da Silva, D. A.; Salman, S.; Bredas, J. L. Effect of Electronic Polarization on Charge-Transport Parameters in Molecular Organic Semiconductors. *J. Am. Chem. Soc.* **2006**, *128*, 9882−9886.
(63) Yamagata, H.; Spano, F. C. Interplay between Intrachain and Interchain Interactions in Semiconducting Polymer Assemblies: The Hj-Aggregate Model. *J. Chem. Phys.* **2012**, *136*, No. 184901.
(64) Silinsh, E. A. *Organic Molecular Crystals, Their Electronic States*; Springer-Verlag: Berlin, 1980.
(65) Ahn, T. S.; Müller, A. M.; Al-Kaysi, R. O.; Spano, F. C.; Norton, J. E.; Beljonne, D.; Brédas, J. L.; Bardeen, C. J. Experimental and Theoretical Study of Temperature Dependent Exciton Delocalization and Relaxation in Anthracene Thin Films. *J. Chem. Phys.* **2008**, *128*, No. 054505.
(66) Spano, F. C. Temperature Dependent Exciton Emission from Herringbone Aggregates of Conjugated Oligomers. *J. Chem. Phys.* **2004**, *120*, 7643−7658.
(67) Sun, H.; Zhao, Z.; Spano, F. C.; Beljonne, D.; Cornil, J.; Shuai, Z.; Bredas, J.-L. Absorption and Emission in Quaterthienyl Thin Films. *Adv. Mater.* **2003**, *15*, 818−821.
(68) Spano, F. C. Absorption and Emission in Oligo-Phenylene Vinylene Nanoaggregates: The Role of Disorder and Structural Defects. *J. Chem. Phys.* **2002**, *116*, 5877−5891.
(69) Engels, B.; Engel, V. The Dimer-Approach to Characterize Opto-Electronic Properties of and Exciton Trapping and Diffusion in Organic Semiconductor Aggregates and Crystals. *Phys. Chem. Chem. Phys.* **2017**, *19*, 12604−12619.
(70) Schubert, A.; Settels, V.; Liu, W.; Würthner, F.; Meier, C.; Fink, R. F.; Schindlbeck, S.; Lochbrunner, S.; Engels, B.; Engel, V. Ultrafast Exciton Self-Trapping Upon Geometry Deformation in Perylene-Based Molecular Aggregates. *J. Phys. Chem. Lett.* **2013**, *4*, 792−796.
(71) Settels, V.; Schubert, A.; Tafipolski, M.; Liu, W.; Stehr, V.; Topczak, A. K.; Pflaum, J.; Deibel, C.; Fink, R. F.; Engel, V.; et al. Identification of Ultrafast Relaxation Processes as a Major Reason for Inefficient Exciton Diffusion in Perylene-Based Organic Semiconductors. *J. Am. Chem. Soc.* **2014**, *136*, 9327−9337.

DOI: 10.1021/acs.jpcc.9b04429
J. Phys. Chem. C 2019, 123, 20567−20578